Appearing in AUTOMATICA, 39(5), MAY 2003, pp. 779-792

Two-Dimensional Loop Shaping ⋆

G.E. Stewart [a,c] , D.M. Gorinevsky [b] , and G.A. Dumont [c]

[a] *Honeywell Industry Solutions, Vancouver Operations, 500 Brooksbank Avenue, North Vancouver, BC, Canada, V7J 3S4.*

[b] *Honeywell Laboratories, One Results Way, Cupertino, CA, USA, 95014.*

[c] *Electrical and Computer Engineering, University of British Columbia, MacLeod Building, 2356 Main Mall Vancouver, BC, Canada V6T 1Z4.*

Abstract

This article considers the design of practical feedback controllers for a class of spatially-distributed processes where the state of a uniform physical substrate is influenced by an array of evenly-distributed, identically-constructed actuators and measured by an array of evenly distributed, identical sensors. A constructive procedure is introduced for designing spatially-distributed feedback controllers with the objective of practical implementation. The full controller design cycle is addressed; including specification, synthesis, and implementation. The proposed design procedure has been field-tested and forms the basis of a software tool that has recently been implemented in a commercial product for the design of industrial paper machine controllers.

Key words: distributed-parameter systems; distributed feedback; control system design; robustness; robust control; robust stability; multidimensional systems.

1 Introduction

This article considers the design of practical feedback controllers for a class of spatially-distributed processes where the state of a uniform physical substrate is influenced by an array of evenly-distributed, identically-constructed actuators and measured by an array of evenly distributed, identical sensors.

⋆ This paper was not presented at any IFAC meeting. Corresponding author G.E. Stewart. Tel. 604-982-3641. Fax 604-980-0120. E-mail Greg.Stewart@Honeywell.com.

We consider processes described by linear time-invariant models that are also spatially-invariant (except possibly near the spatial domain boundaries).

The class of models presented in this work was originally developed to encompass the variety of spatially-distributed processes found on modern industrial paper machines. The physics of these processes include heat transfer and thermal expansion, drying dynamics, fluid flow, and mechanical deformation [37]. Devising a model structure suitable for all of these processes has led to a framework general enough to potentially include a range of spatially-distributed engineering applications:

- Other sheet-forming processes include the formation of plastic film [9,19], and steel making [14,32,33], and are surveyed in [11].
- The growth of semiconductor crystals where arrays of heating elements maintain a uniform temperature distribution throughout the furnace [1].
- Micro-electromechanical systems (MEMS) are an emerging technology in which thousands of tiny actuators distributed over a large structure can be coordinated to achieve global control goals [3,16,31].
- The automated control of a string of vehicles on a highway, known as platoons have been studied in [3,26].
- Mechanical deformation of structures for attenuation of vibration in structures [12], or for low-frequency shape control of optical devices [15].

As stated, the process models treated in this work are linear, time-invariant multivariable systems and therefore could potentially be treated with conventional controller design techniques. However, the problem is complicated by three main issues:

(1) The complexity of the large-scale multivariable processes leads to difficulties in determining practical control objectives for the closed-loop system. In many practical cases, the open-loop process model is ill-conditioned. Even at steady-state, some of its singular values are vanishingly small. Signal norm specifications may be imposed, but the designer must consider the directionality of the process model in order to determine achievable requirements.

(2) The synthesis of a controller for such a large scale system can be intractable even with modern computing power [11]. A process with a few hundred actuators is an order of magnitude larger than the multivariable control systems for which the now-familiar synthesis techniques (for example $\mathcal{H}_2$ and $\mathcal{H}_\infty$) were developed [35,42]. The computational complexity rises quickly with the number of actuators to prohibit the blind application of popular commercially available controller synthesis tools to realistic problems (Section 6.4.2 in [11]).

(3) Finally, when evaluating a design, the practical implementation of a controller must be considered. Many synthesis strategies will result in a fully-centralized controller in which each actuator is required to be connected to

every sensor in the system. While capable of satisfying performance requirements, such a high level of connectivity does not provide a feasible implementation. It may include sensor-actuator pairs that are physically far apart, and the real-time computational complexity becomes important with systems composed of hundreds or thousands of actuators and sensors.

Recognition and exploitation of the near spatially-invariant properties of the processes in question are central to the work presented here. Analogous to time-invariance in dynamical systems, the property of spatial-invariance allows the design problem to be spatially decoupled. This is the key idea of the analysis and synthesis techniques presented in [2,3,6,17]. In [6,17] the spatial-invariance allows the problem to be conveniently presented in a multidimensional state-space format. In [2,3], the large scale multivariable design problem can be decomposed into a family of independent single-input-single-output (SISO) design problems, one for each spatial frequency.

Research in a different direction has simplified controller synthesis algorithms for a more general class of multivariable process models, whose plant model structure is such that the same singular vector matrices may be used to decouple the plant at any temporal frequency. The design of $\mathcal{H}_2$- and $\mathcal{H}_\infty$-optimal controllers again reduces to the design of a family independent of independent SISO controllers - in this case one for each singular value [20].

Plants with symmetric circulant transfer matrices are used throughout the current work and may be interpreted as a special case of either the spatially-invariant structure of [3] or the SVD structure considered in [20]. Controller designs for circulant symmetric plants have been presented in [4,21,25].

The main contribution of this article is a constructive procedure for designing spatially-distributed feedback controllers with the objective of practical implementation. The full controller design cycle, including specification, synthesis, and implementation, is addressed by this procedure.

We introduce the use of the two-dimensional frequency domain at the specification stage prior to controller synthesis. In addition to simplifying the computational complexity of the controller synthesis, many of the familiar concepts from control engineering are present in the two-dimensional frequency domain. For example, in dynamical systems the performance requirements are typically imposed at low temporal frequencies, and robustness requirements are applied at high temporal frequencies. Similarly in the broad class of two-dimensional systems under examination it is found that high performance may be achieved at low spatial and temporal frequencies, while robustness requirements must be imposed at high spatial and temporal frequencies.

Finally, we address two important problems related to the implementation of the designed controller - performance near the boundaries of the spatial do-

main, and its implementation as a low-order, spatially localized control law with a causal time-domain update equation. The incorporation of these issues into the design procedure avoids ad hoc adjustments to a theoretical design when the controller is used in a real-world environment. The design procedure described herein forms the basis of a software package that has been implemented in a commercial product for tuning cross-directional controllers on industrial paper machine systems. Field results demonstrating typical closed-loop performance are described in [37,39,40].

The paper is organized as follows. We introduce the class of process models and controller specifications for performance and implementation in Section 2. Section 3 presents the issues involved in making a spatially-invariant approximation of the problem. Section 3.2 reviews the properties of linear, time and space invariant plants, making such systems attractive for controller design. Section 4 presents the main result with the two-dimensional loop shaping controller design procedure. Section 5 illustrates the application of the design procedure in terms of a realistic but simplified example.

1.1 Notation

This article makes extensive use of banded, symmetric matrices – Toeplitz and circulant. A band-diagonal symmetric Toeplitz matrix of size $n \times n$ with $q < n/2$ degrees of freedom $\bar{a} = [a_1, \ldots, a_q]^T$ is denoted by,

$$A = \mathcal{T}(\bar{a}, n) := \underbrace{\begin{bmatrix} a_1 & a_2 & \cdots & a_q & 0 & \cdots & \cdots & \cdots & 0 \\ a_2 & a_1 & a_2 & \cdots & a_q & 0 & \ddots & \ddots & \vdots \\ \vdots & a_2 & a_1 & a_2 & \vdots & a_q & \ddots & \ddots & \vdots \\ a_q & \cdots & a_2 & a_1 & a_2 & \ddots & \ddots & \ddots & \vdots \\ 0 & a_q & \cdots & a_2 & \ddots & \ddots & \ddots & a_q & 0 \\ \vdots & 0 & a_q & \ddots & \ddots & \ddots & a_2 & \ddots & a_q \\ \vdots & \ddots & \ddots & \ddots & \ddots & a_2 & a_1 & a_2 & \ddots \\ \vdots & \ddots & \ddots & \ddots & a_q & \ddots & a_2 & a_1 & a_2 \\ \vdots & \ddots & \ddots & \ddots & 0 & a_q & \cdots & a_2 & a_1 \\ 0 & \cdots & \cdots & \cdots & \cdots & 0 & a_q & \cdots & a_2 & a_1 \end{bmatrix}}_{n \times n} \tag{1}$$

The related symmetric circulant matrix [7,18] is denoted by,

$$\hat{A} = \mathcal{C}(\bar{a}, n) := \underbrace{\begin{bmatrix} a_1 & a_2 & \cdots & a_q & 0 & \cdots & 0 & a_q & \cdots & a_2 \\ a_2 & a_1 & a_2 & \cdots & a_q & 0 & \ddots & \ddots & \ddots & \vdots \\ \vdots & a_2 & a_1 & a_2 & \vdots & a_q & \ddots & \ddots & \ddots & a_q \\ a_q & \cdots & a_2 & a_1 & a_2 & \ddots & \ddots & \ddots & \ddots & 0 \\ 0 & a_q & \cdots & a_2 & \ddots & \ddots & \ddots & a_q & 0 & \vdots \\ \vdots & 0 & a_q & \ddots & \ddots & \ddots & a_2 & \ddots & a_q & 0 \\ 0 & \ddots & \ddots & \ddots & \ddots & a_2 & a_1 & a_2 & \ddots & a_q \\ a_q & \ddots & \ddots & \ddots & a_q & \ddots & a_2 & a_1 & a_2 & \vdots \\ \vdots & \ddots & \ddots & \ddots & 0 & a_q & \cdots & a_2 & a_1 & a_2 \\ a_2 & \cdots & a_q & 0 & \cdots & 0 & a_q & \cdots & a_2 & a_1 \end{bmatrix}}_{n \times n} \tag{2}$$

Note that the two matrices $\mathcal{T}(\bar{a}, n)$ in (1) and $\mathcal{C}(\bar{a}, n)$ in (2) are the same except for the upper right and lower left corners. This fact will be revisited in Section 3.

2 Problem Statement

This section presents the process model, controller structure specifications, and a collection of practical closed-loop performance specifications.

2.1 Process Model

We consider linear, time-invariant process models of the following form:

$$y(t) = \sum_{i=1}^{m_b} B_i \cdot u(t-i) - \sum_{j=1}^{m_a} A_j \cdot y(t-j) \tag{3}$$

where $y(t) \in \mathcal{R}^n$ is the output vector of n sensor readings at time t, the vector $u(t) \in \mathcal{R}^n$ contains the array of n actuator setpoints at time t, and the coefficients in (3) are band-diagonal symmetric Toeplitz matrices in (1)

$$\begin{aligned} B_i &= \mathcal{T}(\bar{b}_i, n), \qquad \bar{b}_i = [b_1^i, \ldots, b_{n_b}^i]^T \\ A_j &= \mathcal{T}(\bar{a}_j, n), \qquad \bar{a}_j = [a_1^j, \ldots, a_{n_a}^j]^T, \end{aligned} \tag{4}$$

where $i = 1, \ldots, m_b$ and $j = 1, \ldots, m_a$.

The model structure in (3), (4) is motivated by its success in representing spatially-distributed systems. This structure has been used in practically every study of cross-directional profile control on industrial paper machines [11,37]. This model is also common in the spatial and temporal discretization for the explicit solutions of partial differential equations (see Appendix A and [36,41]). Typically the matrices in (3) will have a relatively narrow non-zero band so that $n_b, n_a \ll n$.

The subsequent analysis and design will benefit from the use of a transfer matrix version of (3)–(4). The $\mathcal{Z}$-transform is used to represent the time delays in (3). Writing the factors,

$$B(z) = \sum_{i=1}^{m_b} B_i \cdot z^{-i}, \qquad A(z) = \sum_{j=1}^{m_a} A_j \cdot z^{-j} \tag{5}$$

allows the overall transfer matrix to be written as

$$y(z) = G(z) \cdot u(z), \qquad \text{where} \qquad G(z) = [I + A(z)]^{-1} B(z) \tag{6}$$

where the systems considered in this article are typically modelled with stable transfer matrices $G(z) \in \mathcal{C}^{n \times n}$.

At this point it is worth mentioning that we cannot assume that the transfer matrix $G(z)$ in (3)–(6) is well-conditioned at $\omega = 0$. In fact [9,19] each defend an unusual case that in order to be well-designed, a distributed process is *necessarily* ill-conditioned at steady-state, i.e.

$$\frac{\bar{\sigma}(G(e^{i\omega}))}{\underline{\sigma}(G(e^{i\omega}))} \gg 1, \qquad \text{for } \omega = 0 \tag{7}$$

Processes described by such ill-conditioned transfer matrices require special attention be paid to the directionality of the system when designing a feedback controller [27,34]. This issue will be a central consideration in the development of practical closed-loop specifications (Section 2.3) and must be incorporated into any practical controller design technique.

2.2 Low-Order Controller Implementation

A low-order controller is preferable for practical implementation of feedback control. The spatially-distributed processes described above may have a very

large number of actuators (an industrial example with $n = 226$ actuators is presented in [37,40]). It is inconvenient or even prohibitive to design a controller that links each actuator to every sensor in the array. This has led to the consideration of 'localized' control for spatially-distributed systems [2,3,6].

To address this requirement, we impose the following controller structure,

$$u(t) = \sum_{k=0}^{m_c} C_k \cdot v(t-k) - \sum_{l=1}^{m_d} D_l \cdot u(t-l) \tag{8}$$

where $v(t) = y(t) - r(t) \in \mathcal{R}^n$ represents the deviation of measurement $y(t)$ from the target $r(t)$ and each coefficient matrix is a symmetric Toeplitz structure (1) with,

$$\begin{aligned} C_k &= \mathcal{T}(\bar{c}_k, n), \qquad & \bar{c}_k &= [c_1^k, \ldots, c_{n_c}^k]^T \\ D_l &= \mathcal{T}(\bar{d}_l, n), \qquad & \bar{d}_l &= [d_1^l, \ldots, d_{n_d}^l]^T, \end{aligned} \tag{9}$$

The implementation of the control law in (8)–(9), is more efficient computationally than an equivalent control law constructed from full matrix coefficients. Its implementation requires each actuator to receive information from at most $2n_c - 1$ sensors and $2n_d - 1$ actuators (including itself). This control law is localized and efficient if both $2n_c - 1 \ll n$ and $2n_d - 1 \ll n$.

As with the process model in Section 2.1, the implementation in (8) may be written in transfer matrix notation as,

$$K(z) = [I + D(z)]^{-1} C(z) \tag{10}$$

with the factors,

$$C(z) = \sum_{k=0}^{m_c} C_k \cdot z^{-k}, \qquad D(z) = \sum_{l=1}^{m_d} D_l \cdot z^{-l} \tag{11}$$

Note that the form of localized control suggested by (8) is the same as the process model (3). However, the control law in (8) is causal, while the process model (3) is strictly causal. This is meant to reflect the typical case that discrete time models of dynamical systems do not have a direct feedthrough term. On the other hand, there is at least one industrial controller implementation [37,40] whose implementation is best described with a direct feedthrough term, and the controller formulation in (8) is general enough to include it.

Here we revisit typical multivariable closed-loop performance specifications [8,28,35,42], but with some of the usual assumptions removed. As mentioned above, the array systems (e.g. CD control) can lead to severely ill-conditioned process models, and performance specifications need to be modified to accommodate this limitation.

It is usual to specify the performance requirements on a closed-loop design in the frequency domain. Consider the closed-loop response in the discrete-time frequency domain and consider exciting the system with complex signals of the form (see Section 2.6, of [30]),

$$d(\omega) = [d_1 e^{i(\omega t+\phi_1)}, \ldots, d_n e^{i(\omega t+\phi_n)}]^T \tag{12}$$

where d_j and ϕ_j are real scalars representing magnitude and phase respectively. The discrete time index $t = \{\ldots, -1, 0, 1, 2, \ldots\}$, and $d(\omega)^T$ is the transpose of $d(\omega)$.

The signal norm for $d(\omega)$ in (12) is then given in the frequency domain by the 2-norm,

$$\|d(\omega)\|_2 = \sqrt{d(\omega)^H d(\omega)} = \sqrt{\sum_{j=1}^{n} d_j^2} \tag{13}$$

where $d(\omega)^H$ is the conjugate transpose of $d(\omega)$ in (12). As shown in Table 1, the closed-loop characteristics of the system may be specified in terms of these signal norms and are closely related to the singular value decomposition of the system matrices. For example, the stability robustness to additive unstructured model uncertainty is guaranteed by nominal stability and satisfying the condition,

$$\max_{d_y \neq 0} \frac{\|u\|_2}{\|d_y\|_2} := \bar{\sigma}\left([I - KG]^{-1}K\right) < \frac{1}{\bar{\sigma}(\delta G_A)} \tag{14}$$

where δG_A is a stable transfer matrix perturbing the nominal model as shown in Table 1.

Now consider the output disturbance attenuation in Figure 1. Achieving perfect attenuation means that $\|v\|_2 / \|d_y\|_2 = 0$ in Table 1. This is often applied as a requirement for all d_y in steady-state, at $\omega = 0$. However, if the disturbance d_y aligns with the output singular vector corresponding to $\underline{\sigma}(G)$, then perfect attenuation would require control action of magnitude

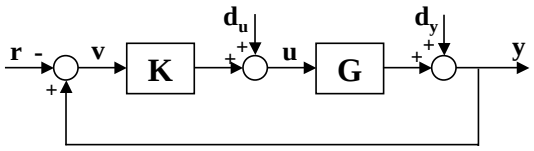

Fig. 1. Control system in positive feedback configuration.

Closed-Loop Characteristic	Signal Ratio	Transfer Matrix
Output disturbance attenuation	$\|v\|_2 \,/\, \|d_y\|_2$	$[I - GK]^{-1}$
Input disturbance attenuation	$\|v\|_2 \,/\, \|d_u\|_2$	$[I - GK]^{-1}G$
Reference tracking	$\|v\|_2 \,/\, \|r\|_2$	$[I - GK]^{-1}$
Limited control action	$\|u\|_2 \,/\, \|d_y\|_2$	$[I - KG]^{-1}K$
Robust stability for $G_p = (I + \delta G_M)G$	$\|y\|_2 \,/\, \|r\|_2$	$GK[I - GK]^{-1}$
Robust stability for $G_p = G + \delta G_A$	$\|u\|_2 \,/\, \|d_y\|_2$	$[I - KG]^{-1}K$

Table 1
Typical systems characteristics for closed-loop design specifications.

$\|u\|_2 \,/\, \|d_y\|_2 = 1/\underline{\sigma}(G)$. Given the ill-conditioned nature of the transfer matrix model in (7), this might yield unacceptably large control action u, and could easily violate the robust stability condition (14).

Closed-loop requirements for performance and robustness are well-known to be in conflict and are therefore typically applied at different temporal frequencies ω of the inputs d_u, d_y, and r in Figure 1. This leads to the familiar open-loop shaping condition that a controller K is to be designed such that the loop gain $\underline{\sigma}(KG)$ (and/or $\underline{\sigma}(K)$) is large at low temporal frequencies and $\bar{\sigma}(KG)$ (and/or $\bar{\sigma}(K)$) is small at high temporal frequencies ω. The discussion above demonstrates that for severely ill-conditioned plants, such as distributed array systems, the performance and robustness specifications must also be separated according to the *directions* of the inputs d_u, d_y, and r in Figure 1. However, a subtle difference should be noted that while the use of linear, time-invariant transfer matrix perturbations to represent model uncertainty does not affect the temporal frequency of the system outputs u, v, and y, it can and will alter their directionality. This fact is reflected in the vector-norm specifications in Table 1 which do not rely on knowledge of the directionality of the true system outputs u, v, and y. We will return to this issue later in this article.

The remainder of this article presents a design strategy that allows the closed-loop specifications such as those in Table 1 to be applied appropriately according to temporal frequency and direction.

3 Controller Design through Circulant Matrix Approximation

The performance characteristics in Table 1 are stated in traditional robust multivariable terms, but cannot generally be solved in a straightforward way for the problem at hand. First, the systems in question may have a large number of inputs and outputs (cross-directional control systems may have up to $n = 300$ actuators), leading to an intractable optimization problem. Second, achieving a controller $K(z)$ with a localized structure as in (8)–(11) is not possible with standard design tools. Finally, the ill-conditioned nature of the plant models $G(z)$ in (3)–(6) requires insight into the singular value decomposition on the part of the designer.

The spatially-distributed system outlined in Section 2 is closely related to a class of spatially-invariant systems, for which design is greatly simplified. This section introduces the approximation of the original problem as a spatially-invariant system. Section 3.2 discusses the features of the spatially-invariant system that simplify the design problem.

3.1 Circulant Approximation of Toeplitz Matrices

Section 2 uses symmetric Toeplitz matrices to describe both the process model $G(z)$ in (3)–(6) and the desired controller structure $K(z)$ in (8)–(11). Systems constructed from such matrices are *almost* spatially-invariant. The analysis is simplified by replacing each of the symmetric Toeplitz matrices (5) with related symmetric circulant matrices in accordance with (1),(2). The difference between a Toeplitz and respective circulant matrix is written as,

$$\delta B := \mathcal{C}(\bar{b}, n) - \mathcal{T}(\bar{b}, n) \tag{15}$$

By inspection, comparing (1) and (2) shows that the matrix δB in (15) is zero everywhere except in the upper-right and lower-left corners.

Transition to the circulant matrices means that we approximate the process model in (6) using periodic boundary conditions as,

$$\hat{G}(z) = [I + \hat{A}(z)]^{-1}\hat{B}(z) \tag{16}$$

where the symmetric circulant transfer matrix factors are created according to (15),

$$\hat{B}(z) := \sum_{k=1}^{m_b} \hat{B}_k \cdot z^{-k}, \qquad \hat{A}(z) := \sum_{l=1}^{m_a} \hat{A}_l \cdot z^{-l} \tag{17}$$

A similar operation is used to construct a controller $\hat{K}(z)$ with symmetric circulant factors $\hat{C}(z)$ and $\hat{D}(z)$ from the symmetric Toeplitz matrix factors $C(z)$ and $D(z)$ in (11).

The corresponding 'true' system has band-diagonal transfer matrices $A(z)$, $B(z)$, $C(z)$, $D(z)$ which are related to the symmetric circulant transfer matrices $\hat{A}(z)$, $\hat{B}(z)$, $\hat{C}(z)$, $\hat{D}(z)$, where the transfer matrix perturbations are each,

$$\delta B(z) = \sum_{i=1}^{m_b} \delta B_i \cdot z^{-i}, \tag{18}$$

where δB_i is described in (15).

Since each transfer matrix factor $A(z)$, $B(z)$, $C(z)$, $D(z)$ in (5), (11) is an FIR polynomial in z^{-1} (with constant matrix coefficients), then trivially each transfer matrix is stable (although the plant model $G(z)$ in (6) and the controller $K(z)$ in (10) may not be stable). Also, since the perturbations in (18) are also FIR polynomials in z^{-1}, then the circulant symmetric factors $\hat{A}(z)$, $\hat{B}(z)$, $\hat{C}(z)$, $\hat{D}(z)$ are stable as well. This allows the expression of the internal stability of the closed-loop in terms of the simple transfer matrix factors [42].

The internal stability of the 'true' closed-loop system is equivalent to

$$\begin{aligned} L(z) &:= \begin{bmatrix} I + D(z) & C(z) \\ B(z) & I + A(z) \end{bmatrix} \\ &= \begin{bmatrix} I + \hat{D}(z) & \hat{C}(z) \\ \hat{B}(z) & I + \hat{A}(z) \end{bmatrix} - \begin{bmatrix} \delta D(z) & \delta C(z) \\ \delta B(z) & \delta A(z) \end{bmatrix} \end{aligned} \tag{19}$$

being invertible for all $|z| \geq 1$, where the first term in (19) refers to the circulant system and the second term contains the perturbations as in (18).

As will be discussed in Section 3.2, it is far simpler to analyze the stability of a system composed of circulant, rather than Toeplitz, transfer matrices. A conservative, but computationally attractive approach may be found by appealing to robust control theory for the stability of feedback systems with perturbations. A sufficient condition for the internal stability of the true system defined by $L(z)$ in (19) follows from the small gain theorem. The closed-loop system with $L(z)$ is stable if the circulant system is stable and

$$\left\| \begin{bmatrix} \delta D(z) & \delta C(z) \\ \delta B(z) & \delta A(z) \end{bmatrix} \cdot \begin{bmatrix} I + \hat{D}(z) & \hat{C}(z) \\ \hat{B}(z) & I + \hat{A}(z) \end{bmatrix}^{-1} \right\|_{\infty} < 1 \tag{20}$$

The systems under consideration are typically described by transfer matrices with relatively narrow non-zero bands. For example, [37] contains an industrial example in which the Toeplitz symmetric transfer matrix $B(z)$ is $n \times n$ with $n = 226$ but has only 5 non-zero diagonals. This leads to a large number of zero rows and columns in the perturbations (15) which may be removed to reduce the size of the computation without affecting the result in (20). The incorporation of spatial boundary conditions in a consistent manner is the subject of active research and is progressing in [24,29,38].

3.2 Controller Design for a Circulant System

All symmetric circulant systems of the same size are diagonalized with the *same* unitary matrix F (defined as the real Fourier matrix in Appendix B in (B.4)) by pre- and post-multiplication by $F(\cdot)F^T$. Since $F^T = F^{-1}$, then this is the eigenvector matrix. This condition also implies that the same eigenvector matrix F will diagonalize symmetric circulant transfer matrices such as $\hat{G}(z)$ and $\hat{K}(z)$ in (16)–(17) above at all temporal frequencies $\omega \in [-\pi, \pi]$.

For example, the eigenvalues of the transfer matrix $\hat{G}(z)$ in (16) are given by,

$$F \cdot \hat{G}(z) \cdot F^T = \mathrm{diag}\{\hat{g}(\nu_1, z), \ldots, \hat{g}(\nu_n, z)\}, \tag{21}$$

where the variable ν_j indicates the spatial frequency of the j^{th} spatial mode and is given by $\nu_j = 2\pi(j-1)/n$ (see Appendix B). The individual SISO subsystems (eigenvalues of $\hat{G}(z)$) are given by,

$$\hat{g}(\nu_j, z) = \frac{\hat{b}(\nu_j, z)}{1 + \hat{a}(\nu_j, z)} \tag{22}$$

$$\hat{b}(\nu_j, z) = \sum_{k=1}^{m_b} \hat{b}_k(\nu_j) \cdot z^{-k}, \qquad \hat{a}(\nu_j, z) = \sum_{l=1}^{m_a} \hat{a}_l(\nu_j) \cdot z^{-l} \tag{23}$$

due to the fact that

$$F \cdot \hat{G}(z) \cdot F^T = [I + F \cdot \hat{A}(z) \cdot F^T]^{-1} F \cdot \hat{B}(z) \cdot F^T \tag{24}$$

$$F \cdot \hat{B}(z) \cdot F^T = F \left(\sum_{k=1}^{m_b} \hat{B}_k \cdot z^{-k} \right) \cdot F^T$$

$$= \sum_{k=1}^{m_b} \text{diag}\{\hat{b}_k(\nu_1), \ldots, \hat{b}_k(\nu_n)\} \cdot z^{-k} \tag{25}$$

For a controller (10) constructed from symmetric circulant matrix factors, then a similar operation can be used to obtain,

$$\hat{k}(\nu_j, z) = \frac{\hat{c}(\nu_j, z)}{1 + \hat{d}(\nu_j, z)} \tag{26}$$

for spatial frequencies $\nu_j \in \{\nu_1, \ldots \nu_n\}$.

The simultaneous decoupling of the process model and feedback controller in (22) and (26) provides an advantage in the design of the feedback controllers as described next.

3.3 Analysis and Synthesis

The singular values of a symmetric circulant matrix are equal to the magnitude of its eigenvalues [7]. This property is rare in multivariable control systems, and has the advantage of simplifying the design problem. This section presents results from [3,21] indicating that, for a wide variety of practical performance criteria, the design of a large $n \times n$ multivariable controller $\hat{K}(z)$ for the class of symmetric circulant dynamical systems at hand, is equivalent to designing a family of n SISO controllers $\hat{k}(\nu_j, z)$.

The general statement of the feedback control problem is: given exogenous inputs $w(z)$ to a system, find a controller which uses sensor data $y(z)$ to calculate actuator inputs $u(z)$ which counteract the influence of $w(z)$ on the signal $e(z)$ [35]. The problem of keeping the generalized error $e(z)$ small is often quantified in terms of a norm on the closed-loop transfer function from the inputs $w(z)$ to $e(z)$ as in Table 1. A generalized plant may be used to describe the path from the exogenous inputs to the outputs of a feedback control system [5,35].

A generalized plant $P(z)$ and feedback controller are introduced such that

$$\begin{bmatrix} e(z) \\ v(z) \end{bmatrix} = P(z) \begin{bmatrix} w(z) \\ u(z) \end{bmatrix}, \qquad u(z) = K(z)v(z) \tag{27}$$

where $P(z)$ contains the open-loop plant $\hat{G}(z)$ in (16) and all transfer matrices associated with disturbances and performance weights. The transfer matrix

$K(z)$ describes the feedback controller where $u(z)$ is the control signal and $v(z)$ is the feedback signal.

Theorem 1 *(cf. [3,21,37])***(Controller Structure)** *If the generalized plant $P(z)$ in (27) is composed of symmetric circulant transfer matrices, and if there exists a controller such that the closed-loop is any of (i) $\mathcal{H}_2$ optimal, or (ii) $\mathcal{H}_\infty$ optimal, or (iii) $\mathcal{H}_\infty$ admissible, then there exists a symmetric circulant controller $\hat{K}(z)$ in (27) that satisfies the respective criterion.*

Proof. See [3,21,37].

This existence theorem is then augmented with a constructive theorem which greatly simplifies the synthesis of such controllers.

Theorem 2 *(cf. [3,21])* **(Controller Synthesis)** *Feedback controllers satisfying any one of the objectives in Theorem 1 may be synthesized as a family of SISO controllers $\hat{k}(\nu_j, z)$, independently for each spatial frequency $\nu_j \in \{\nu_1, \ldots, \nu_n\}$, then constructing the multivariable controller*

$$\hat{K}(z) = F^T \cdot \mathrm{diag}\{\hat{k}(\nu_1, z), \ldots, \hat{k}(\nu_n, z)\} \cdot F \tag{28}$$

Furthermore, for symmetric circulant systems, the eigenvalues occur in pairs and we only need to design controllers for $\nu_j \in \{\nu_1, \ldots, \nu_p\}$ where $p = (n+2)/2$ if n is even, and $p = (n+1)/2$ if n is odd. The remaining $n - p$ controllers are constructed with $\hat{k}(\nu_i, z) = \hat{k}(\nu_{2+n-i}, z)$ for $p + 1 \leq i \leq n$.

Proof. See [3,21].

3.4 Practical Controller Implementation

The previous subsection summarized the advantages provided by symmetric circulant systems to the designer for the synthesis of feedback controllers. In this section we consider the implementation of the controller as a time domain update form with a localized controller structure according to Section 2.2. Theorem 3 maps out a factorization that will result in an implementable format. Theorem 4 presents a result that allows a localized controller to be fit to a fully centralized controller.

Theorem 3 (Controller Implementation) *If a family of causal finite-order rational SISO transfer functions $\hat{k}(\nu_j, z)$ for $\nu_j \in \{\nu_1, \ldots, \nu_n\}$ has been synthesized (for example satisfying Theorem 2), then the full MIMO controller $\hat{K}(z)$ in (28) can be implemented in the discrete-time domain as the update,*

$$u(t) = \sum_{k=0}^{m_c} \hat{C}_k \cdot v(t-k) - \sum_{l=1}^{m_d} \hat{D}_l \cdot u(t-l) \tag{29}$$

with finite m_c and m_d and real symmetric circulant matrices $\hat{C}_k$ and $\hat{D}_l$.

Proof. Since $\hat{k}(\nu_j, z)$ is causal and finite order then we can write,

$$\hat{k}(\nu_j, z) = \frac{\sum_{k=0}^{m_c} \hat{c}_k(\nu_j) \cdot z^{-k}}{1 + \sum_{l=1}^{m_d} \hat{d}_l(\nu_j) \cdot z^{-l}} \tag{30}$$

The matrices in (29) are constructed with an inverse Fourier transform,

$$\hat{C}_k = F^T \cdot \mathrm{diag}\{\hat{c}_k(\nu_1), \ldots, \hat{c}_k(\nu_n)\} \cdot F \tag{31}$$

for $k = 0, \ldots, m_c$. Similar expressions hold for $\hat{D}_l$ for $l = 1, \ldots, m_d$. $\diamondsuit$

In general, a symmetric circulant matrix that has been constructed frequency-by-frequency in terms of its spectrum $\hat{c}(\nu_j)$ for $j = 1, \ldots, n$ and the inverse Fourier transform (31) will result in full (as opposed to banded) matrices $\hat{C}_k$ and $\hat{D}_l$ in (29). The specification in Section 2.2 states the preference for low-order controllers, and we need to implement the control using matrix factors in (29) where,

$$\hat{C}_r = \mathcal{C}(\bar{c}, n), \qquad \bar{c} = [c_1, \ldots, c_{n_c}]^T, \tag{32}$$

with $2n_c - 1 \ll n$ for a reduced order matrix in (2).

The following Theorem illustrates a result that will be used to approximate a full circulant matrix with a low-order, banded symmetric circulant matrix.

Theorem 4 (Controller Reduction) *Let $\hat{c}(\nu_j)$ with $j = 1, \ldots, n$ be an eigenvalue spectrum of a symmetric circulant matrix with $\hat{c}(\nu_i) = \hat{c}(\nu_{2+n-i})$ for $p+1 \leq i \leq n$ (where $p = (n+2)/2$ if n is even, and $p = (n+1)/2$ if n is odd) and eigenvector matrix F in (B.4). Let $\hat{c}_r(\nu_j)$ be the spectrum of eigenvalues corresponding to a reduced matrix $\hat{C}_r$ in (32). Then the least squares approximation*

$$J := \min_{\bar{c}} \sum_{j=1}^{n} [\hat{c}_r(\nu_j) - \hat{c}(\nu_j)]^2 \tag{33}$$

is achieved with $\bar{c}_{opt} = [c_1, \ldots, c_{n_c}]^T$ in (32) with coefficients given by,

$$c_i = \frac{1}{n}\sum_{j=1}^{n} \hat{c}(\nu_j)\cdot\cos[(i-1)\cdot\nu_j], \qquad i = 1,\ldots,n_c \tag{34}$$

Furthermore, if $n_c = p$ then the fit (34) results in $J = 0$ in (33) and $\hat{C}_r = \hat{C}$.

Proof. See Appendix C for the proof. $\diamondsuit$

The optimization index in (33) indicates that the reduced-order controller's matrix coefficients will approximate the coefficients of the original high-order controller. Strictly speaking, we are interested in controller reduction techniques that preserve the closed-loop stability and performance of the high-order controller. However, this is a much more difficult problem and currently remains the subject of active research. The advantage of the method presented in Theorem 4 is that it is computationally efficient, results in acceptable low-order controllers in the majority of practical cases, and will converge to the original high-order controller if required.

Equation (33) allows the computation of the controller coefficients $\bar{c} = [c_1,\ldots,c_{n_c}]^T$ in (32) *directly* from the spectra $\hat{c}(\nu_j)$ synthesized using Theorem 2. Thus Theorem 4 allows avoiding the construction of (potentially large) $n \times n$ matrices and reduces the computational load on the design of reduced matrices as in (32).

There is a potential tradeoff between controller performance and controller localization in the proposed design technique. If each of the n SISO controllers has been designed frequency-by-frequency according to Theorem 2, then the use of a reduction technique such as Theorem 4 may degrade the closed-loop performance from the original high-order (centralized) design. However, the performance of the centralized controller may be recovered completely by allowing the spatial order $n_c \to p$ in Theorem 4. If this is done for each of the coefficient matrices $\hat{C}_k$ and $\hat{D}_l$ in (29), then the controller reverts to its full order and converges to the high performance of the original design. It should be noted that in practice we typically get 'acceptable' performance with $n_c \ll p$. Section 5 provides an example with $n = 101$ actuators where $p = 51$ and acceptable performance is achieved with spatial order $n_c = n_d = 5$ for each of the controller's coefficients.

3.5 Physical Insight

The singular vectors of symmetric circulant matrices allow an intuitive physical interpretation as harmonic functions of the spatial variable (the rows of the real Fourier matrix F in (B.4)). This fact allows an intuitive physical interpretation of the multivariable system considered herein in terms of its spatial and temporal frequency response. Consider for example, the fact that the process

models for the spatially-distributed systems describing web-forming processes are typically ill-conditioned [11,19,23,37].

The singular values of the circulant system $\hat{G}(e^{i\omega})$ are given by the magnitude of the eigenvalues $|\hat{g}(\nu_j, e^{i\omega})|$ and a typical industrial papermaking example is illustrated in Figure 2. The singular values are plotted in order of increasing spatial frequency $\nu_j = 2\pi(j-1)/n$. Figure 2 illustrates a characteristic that is common to the vast majority of industrial cross-directional processes - the singular values that correspond to high spatial frequencies have a very small gain. The gain of most CD processes rolls off as a function of both spatial and temporal frequencies.

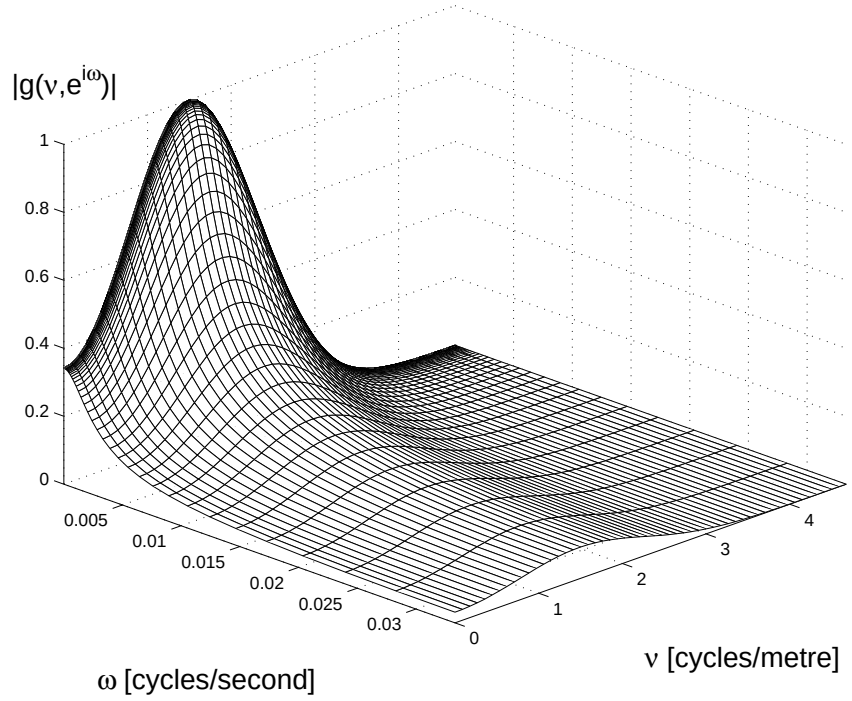

Fig. 2. Typical two-dimensional high frequency gain roll-off (data from the industrial system described in [39,40]).

Gain roll-off at high temporal frequencies is familiar from dynamical systems where it is now understood to be a feature of all realistic models of physical devices. An analogous feature appears to be present in many spatially distributed systems that model physical processes [3,37]. In fact, in [9,10,19] it is explained that gain roll-off at high spatial frequencies is an important feature required in practical control systems which are controlled by a spatially discrete set of actuators.

Ill-conditioned multivariable plants are considered to be difficult to control [27,34]. The advantage of interpreting the ill-conditioning as gain roll-off at high spatial frequencies lies in the fact that frequency domain design methods

Closed-Loop Characteristic	Open-Loop Specification	Typically Applied
Output disturbance attenuation	$\lvert\hat{g}\hat{k}\rvert$ large, where $\lvert\hat{g}\rvert$ large	low ω and ν
Input disturbance attenuation	$\lvert\hat{k}\rvert$ large, where $\lvert\hat{g}\rvert$ large	low ω and ν
Reference tracking	$\lvert\hat{g}\hat{k}\rvert$ large, where $\lvert\hat{g}\rvert$ large	low ω and ν
Limited control action	$\lvert\hat{k}\rvert$ small, where $\lvert\hat{g}\rvert$ small	high ω and ν
Robust stability for $G_p = (I + \delta G_M)\hat{G}$	$\lvert\hat{g}\hat{k}\rvert$ small, where $\bar{\sigma}(\delta G_M) \approx 1$ and/or $\bar{\sigma}(\delta G_M) \geq 1$	high ω and ν
Robust stability for $G_p = \hat{G} + \delta G_A$	$\lvert\hat{k}\rvert$ small, where $\lvert\hat{g}\rvert \approx \bar{\sigma}(\delta G_A)$ and/or $\lvert\hat{g}\rvert \leq \bar{\sigma}(\delta G_A)$	high ω and ν

Table 2
Closed-loop design specifications of Table 1 rewritten for practical two-dimensional control.

are very well-developed for addressing gain roll-off at high temporal frequencies in dynamical systems. Section 4 extends these loop shaping design techniques to the two-dimensional frequency domain and presents the controller specifications in Section 2.3 in terms of both spatial and temporal frequencies.

4 Two-Dimensional Loop Shaping

Typical closed-loop objectives imposed on the design of a feedback controller are summarized in Table 1. It is well-known that these are in conflict and cannot be satisfied simultaneously [35,42]. Traditionally this conflict is avoided by the fact that these objectives are generally in different temporal frequency ranges. The performance criteria can be satisfied for large model gain and small relative uncertainty, typically at low frequencies ω. The robustness criteria are then required for small model gain and large relative uncertainty, typically at high frequencies ω.

In Section 3, the two-dimensional frequency decomposition of these spatially-distributed systems was presented. This decomposition has a direct impact on the closed-loop specifications of Table 1. Take for example the specification on robust stability for additive unstructured uncertainty (as in (14)),

$$G_p = \hat{G} + \delta G_A, \quad \text{with } \bar{\sigma}(\delta G_A) < \beta \tag{35}$$

where the perturbation δG_A is unstructured and is not necessarily a symmetric circulant matrix as is $\hat{G}$. Robust stability with the feedback controller $\hat{K}$ is achieved with a nominally stable closed-loop and the condition,

$$\bar{\sigma}\left([I - \hat{K}\hat{G}]^{-1}\hat{K}\right) < \frac{1}{\beta} \tag{36}$$

for all $\omega \in [-\pi, \pi]$. If the plant model $\hat{G}$ and feedback controller $\hat{K}$ are symmetric circulant transfer matrices, then the singular values are given by the magnitude of the spatial frequency components and the multivariable condition (36) reduces to

$$\left|\frac{\hat{k}(\nu_j, e^{i\omega})}{1 - \hat{g}\hat{k}(\nu_j, e^{i\omega})}\right| < \frac{1}{\beta} \tag{37}$$

for all temporal frequencies $\omega \in [-\pi, \pi]$ and each spatial frequency $\nu_j \in \{\nu_1, \ldots, \nu_n\}$. Condition (37) is satisfied naturally when $|\hat{k}(\nu_j, e^{i\omega})|$ is large and $|\hat{g}(\nu_j, e^{i\omega})| > \beta$ typically at low temporal and spatial frequencies. However, at frequencies where $|\hat{g}(\nu_j, e^{i\omega})|$ is small,

$$\left|\frac{\hat{k}(\nu_j, e^{i\omega})}{1 - \hat{g}\hat{k}(\nu_j, e^{i\omega})}\right| \approx |\hat{k}(\nu_j, e^{i\omega})| \tag{38}$$

and an upper bound must be imposed on the gain of the controller $|\hat{k}(\nu_j, e^{i\omega})|$ in order to satisfy condition (37). Figure 2 illustrates the typical case where the gain of the plant model $|\hat{g}(\nu_j, e^{i\omega})|$ rolls off for high spatial and temporal frequencies.

One may apply an argument similar to (35)–(38) to each of the closed-loop specifications in Table 1 to obtain the open-loop approximations for in Table 2 for these symmetric circulant systems. The results are analogous to traditional loop shaping in which closed-loop specifications lead to approximate open-loop specifications that may be summarized by achieving high loop gain and controller gain at low temporal frequencies and low loop gain and controller gain at high temporal frequencies. In the case of two-dimensional loop shaping, Table 2 indicates that the specifications may be separated in terms of low and high temporal and *spatial* frequencies. This design tradeoff is demonstrated next.

Good performance requires that the loop gain and/or controller gain be lower-bounded

$$|\hat{g}(\nu_j, e^{i\omega})\hat{k}(\nu_j, e^{i\omega})| > w_l, \qquad \text{and/or} \qquad |\hat{k}(\nu_j, e^{i\omega})| > h_l \tag{39}$$

typically applied at low spatial and temporal frequencies $\{\nu_j, \omega\} \in \Omega_l$.

The robust stability and limited control action specifications require that the loop gain and/or controller gain be upper-bounded

$$|\hat{g}(\nu_j, e^{i\omega})\hat{k}(\nu_j, e^{i\omega})| < w_h, \qquad \text{and/or} \qquad |\hat{k}(\nu_j, e^{i\omega})| < h_h \tag{40}$$

typically applied at high spatial and temporal frequencies $\{\nu_j, \omega\} \in \Omega_h$. (Note that for practical control design, robustness and performance specifications are separated with $w_h \ll w_l$ and $h_h \ll h_l$ in (39) and (40).)

The loop shaping conditions (39) and (40) are graphically illustrated for the loop gain conditions in the contour plot in Figure 3. It follows that two-dimensional loop shaping requires to design $\hat{k}(\nu_j, z)$ such that the contours $|\hat{g}(\nu_j, e^{i\omega})\hat{k}(\nu_j, e^{i\omega})| = w_l$ and $|\hat{g}(\nu_j, e^{i\omega})\hat{k}(\nu_j, e^{i\omega})| = w_h$ avoid the shaded areas Ω_l and Ω_h. The performance condition (39) is satisfied if the $|\hat{g}\hat{k}| = w_l$ contour does not intersect the set Ω_l. The robustness condition (40) is satisfied if the $|\hat{g}\hat{k}| = w_h$ contour does not intersect the set Ω_h.

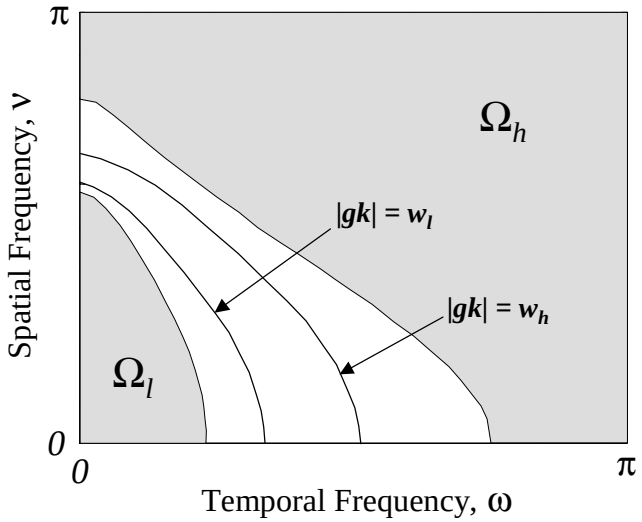

Fig. 3. Contour plot in $\omega\nu$ with sets Ω_l and Ω_h represented by the shaded areas. The contours $|\hat{g}\hat{k}| = w_l$ and $|\hat{g}\hat{k}| = w_h$, illustrate a design that is successfully trading off and meeting the loop gain requirements in (39) and (40).

Constructive Design Algorithm

(1) *Diagonalize the problem.* Motivated by Theorem 1, using Section 3, approximate the spatial boundary conditions and write $\hat{G}(z)$ and $\hat{K}(z)$ as the decoupled family $\hat{g}(\nu_j, z)$ and $\hat{k}(\nu_j, z)$ for $\nu_j \in \{\nu_1, \ldots, \nu_n\}$.

(2) *Controller synthesis.* According to Theorem 2, for each SISO plant $\hat{g}(\nu_j, z)$ synthesize a SISO controller $\hat{k}(\nu_j, z)$ in Step 1 to satisfy closed-loop requirements for each $\nu_j \in \{\nu_1, \ldots, \nu_n\}$.

(3) *Controller reduction.*[1] Factor the family of SISO controllers such that $\hat{k}(\nu_j, z) = \hat{c}(\nu_j, z)/[1 + \hat{d}(\nu_j, z)]$ with $\hat{c}(\nu_j, z) = \sum_{k=0}^{m_c} \hat{c}_k(\nu_j) \cdot z^{-k}$ and $\hat{d}(\nu_j, z) = \sum_{l=0}^{m_d} \hat{d}_l(\nu_j) \cdot z^{-l}$.

[1] In [6] a synthesis technique is proposed with which one can directly design low-order distributed controllers, potentially eliminating this reduction step.

Select the degree of controller localization n_c and n_d and apply Theorem 4 to coefficients $\hat{c}_k(\nu_j)$ and $\hat{d}_l(\nu_j)$, to reduce the spatial order of the controller generated in Step 2 and obtain coefficients $\bar{c}_k \in \mathcal{R}^{n_c}$ and $\bar{d}_l \in \mathcal{R}^{n_d}$. If necessary, increase n_c and n_d until the reduced-order controller $\hat{K}_r(z)$ satisfies the loop shaping design requirements.

(4) *Construct* the reduced matrices $\hat{C}_k = \mathcal{C}(\bar{c}_k, n)$ and $\hat{D}_l = \mathcal{C}(\bar{d}_l, n)$ in (9) according to Theorem 3 using the coefficients from Step 3.

(5) *Check* the internal stability of the associated Toeplitz system (e.g. condition (20)), and implement the control using band-diagonal Toeplitz factors $C_k = \mathcal{T}(\bar{c}_k, n)$ and $D_l = \mathcal{T}(\bar{d}_l, n)$ in (8). If internal stability is not satisfied, the designer is obliged to return to the controller synthesis step to achieve acceptable margins.

5 Example

A detailed account of an industrial application of this technique can be found in [37,40]. For now we will present an abstracted example so as to concentrate on the above concepts.

The design steps outlined above are presented in terms of a simple, but realistic numerical example taken from the papermaking industry. To manufacture high-quality paper for printing, it is important that variations in the caliper (i.e. thickness) of a sheet of paper be kept as small as possible [22,37].

In this industrial process application, the caliper of a 7.85m wide sheet of paper is controlled by feeding the paper sheet through (at least) two counter-rotating rollers. The caliper of the paper will be altered by the pressure between these two rollers. The pressure exerted upon the paper sheet is locally controlled by an array of $n = 101$ identically designed actuators, evenly spaced on 7.6cm centres. The induction heating actuators increase (decrease) the pressure by locally heating (cooling) one of the rollers. The corresponding thermal expansion (shrinkage) of the roller causes the pressure to increase (decrease), thereby decreasing (increasing) the caliper of the pressed paper. The process model is given by,

$$y(t) = B \cdot u(t-2) - A \cdot y(t-1) \tag{41}$$

where $A, B \in \mathcal{R}^{101\times 101}$ are symmetric Toeplitz matrices $B = \mathcal{T}(\bar{b}, 101)$ and $A = \mathcal{T}(\bar{a}, 101)$ with,

$$\overline{b} = \begin{bmatrix} -0.0381 \\ -0.0240 \\ 0.0013 \\ 0.0126 \\ 0.0092 \\ 0.0035 \end{bmatrix}, \qquad \overline{a} = \begin{bmatrix} -0.4689 \\ -0.2433 \\ 0.0024 \\ 0.0196 \end{bmatrix} \tag{42}$$

Step 1 in the loop shaping design algorithm is to form an approximation of this system with periodic boundary conditions, $\hat{B} = \mathcal{C}(\bar{b}, 101)$ and $\hat{A} = \mathcal{C}(\bar{a}, 101)$ as shown in Section 3.1. Then we can write the eigenvalue spectrum of the symmetric circulant process model as,

$$\hat{g}(\nu_j, z) = \frac{\hat{b}(\nu_j) z^{-2}}{1 + \hat{a}(\nu_j) z^{-1}} \tag{43}$$

for each spatial frequency $\nu_j \in \{\nu_1, \ldots, \nu_{101}\}$ we have a plant model with first order and deadtime dynamics, the gain $\hat{b}(\nu_j)$ and pole $\hat{a}(\nu_j)$ are each a function of the spatial frequency ν_j.

Step 2 in the design is the synthesis of a SISO controller, one for each spatial frequency. Here we select a $\mathcal{H}_2$ performance index,

$$J(\nu_j) = \left\| w_e(\nu_j, z) \cdot \frac{1}{1 - \hat{g}\hat{k}(\nu_j, z)} \right\|_2^2 + \left\| w_u(\nu_j, z) \cdot \frac{\hat{k}(\nu_j, z)}{1 - \hat{g}\hat{k}(\nu_j, z)} \right\|_2^2 \tag{44}$$

which is easily solved for a SISO controller

$$\hat{k}(\nu_j, z) = \frac{\hat{c}_1(\nu_j) z^{-1} + \hat{c}_2(\nu_j) z^{-2} + \hat{c}_3(\nu_j) z^{-3}}{1 + \hat{d}_1(\nu_j) z^{-1} + \hat{d}_2(\nu_j) z^{-2} + \hat{d}_3(\nu_j) z^{-3} + \hat{d}_4(\nu_j) z^{-4}} \tag{45}$$

for each spatial frequency $\nu_j \in \{\nu_1, \ldots, \nu_{51}\}$, using the Robust Control Toolbox [5] function *dh2lqg.m*. As discussed in Theorem 2, the remaining $n - p = 50$ controllers are constructed with $\hat{k}(\nu_j, z) = \hat{k}(\nu_{2+n-j}, z)$ for spatial frequencies $\nu_j \in \{\nu_{52}, \ldots, \nu_{101}\}$. The low-pass filter $w_e(\nu_j, z)$ and high-pass filter $w_u(\nu_j, z)$ are low-order transfer functions [2] designed to shape the frequency response of the loop gain (see Figure 4).

[2] The specific numerical values of the weights w_e and w_u in (44) are unimportant to the presentation of the design algorithm and are omitted for space and continuity.

The performance/robustness trade off may be viewed in terms of the loop gain $|\hat{g}\hat{k}(\nu_j, e^{i\omega})|$ in Figure 4. In order to guarantee attenuation of over 80% of disturbances (i.e. $|1-\hat{g}\hat{k}|^{-1} < -14$dB) at low frequencies, the loop gain is required to satisfy $|\hat{g}\hat{k}| > 6.0$ (15.6dB) for the set of low frequencies $\{\nu, \omega\} \in \Omega_l$ as depicted in Figure 4. The robustness requirement is taken to be $|\hat{g}\hat{k}| < 0.1$ (-20dB) for the set of high frequencies $\{\nu, \omega\} \in \Omega_h$ as indicated in Figure 4.

Since each of the coefficient spectra $\hat{c}_i(\nu_j)$ and $\hat{d}_l(\nu_j)$ in (45) corresponds to a full symmetric circulant matrix, Step 3 of the design allows to reduce the order of the controller using Theorem 4. For simplicity we let the 'numerator' spatial order equal the 'denominator' spatial order and define an overall order $n_k = n_c = n_d$. Figure 4 illustrates the results where the matrices are reduced in turn to $n_k = 1$ (decentralized control), $n_k = 5$, and $n_k = 11$. It can be seen that the full reduction to $n_k = 1$ results in very poor reproduction of the optimal loop gain (indicated with the dashed lines). The optimal loop gain is approached as the controller order n_k is increased. A controller with order $n_k = 11$ provides close to the true optimal loop gain which has $n_k = 51$ (see Theorem 4).

Step 4 of the design is to create the matrix factors required for the implementation of the low-order controller according to Theorem 3

$$\begin{aligned} u(t) = \hat{C}_1 \cdot y(t-1) + \ldots + \hat{C}_3 \cdot y(t-3) \\ - \hat{D}_1 \cdot u(t-1) - \ldots - \hat{D}_4 \cdot u(t-4) \end{aligned} \tag{46}$$

where the $n_k = 5$ coefficients of the symmetric circulant controller matrices in (46) are extracted from the spectra according to Theorem 4 as

$$\{\overline{c}_1, \overline{c}_2, \overline{c}_3\} = \begin{bmatrix} 0.8760 & -0.9541 & 0.1834 \\ 0.5360 & -0.5592 & 0.0725 \\ 0.0389 & 0.0432 & -0.1011 \\ -0.0043 & 0.1387 & -0.1323 \\ 0.1361 & -0.0341 & -0.0685 \end{bmatrix},$$

$$\{\overline{d}_1, \overline{d}_2, \overline{d}_3, \overline{d}_4\} = \begin{bmatrix} -1.6776 & 0.8767 & -0.2099 & 0.0244 \\ -0.0508 & 0.1334 & -0.0987 & 0.0131 \\ 0.0769 & -0.0898 & 0.0210 & -0.0076 \\ 0.0114 & -0.0181 & 0.0227 & -0.0164 \\ -0.0206 & 0.0269 & 0.0037 & -0.0108 \end{bmatrix}, \tag{47}$$

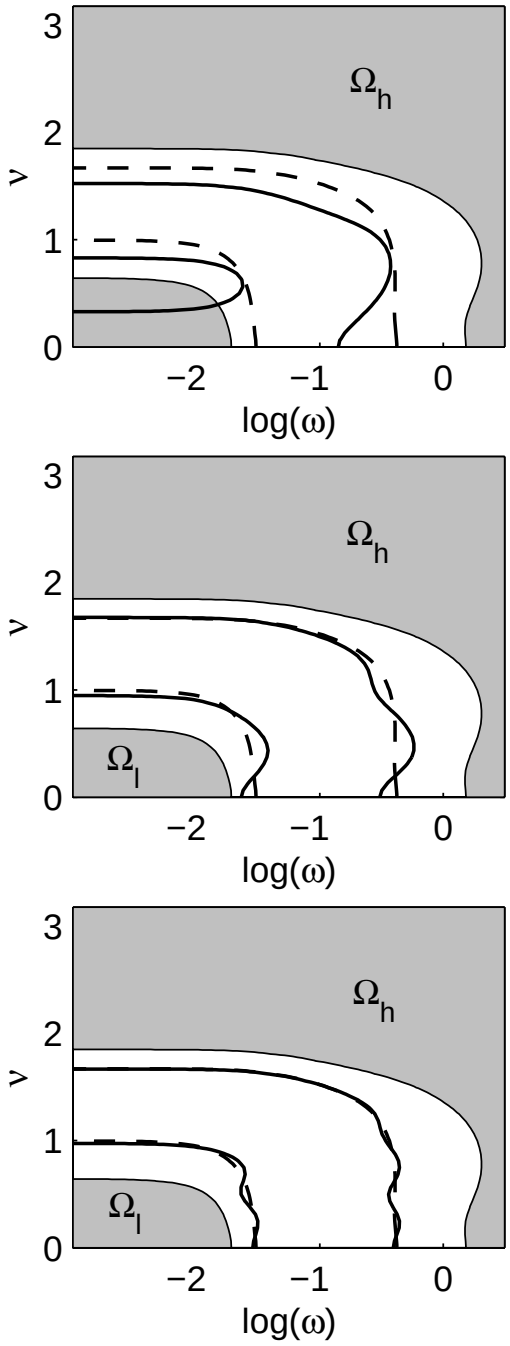

Fig. 4. Contour plots of the loop gain $|\hat{g}\hat{k}| = 6.0$ and $|\hat{g}\hat{k}| = 0.1$. The original, high-order controller is given by the dashed lines, the reduced controller is indicated with solid lines. (a) The fully decentralized controller with $n_k = 1$ for all matrices $\hat{C}_k$ and $\hat{D}_l$ violates the low frequency performance constraint since the contour $|\hat{g}\hat{k}| = 6.0$ intersects the set Ω_l, (b) Low order design $n_k = 5$ is sufficient, (c) High-order $n_k = 11$ approaches original performance.

where $\hat{C}_k = \mathcal{C}(\bar{c}_k, n)$ for $k = 1, 2, 3$ and $\hat{D}_l = \mathcal{C}(\bar{d}_l, n)$ for $l = 1, \ldots, 4$ in (46),(47).

Finally, Step 5 requires that the 'true' spatial boundary conditions be implemented, and here it is required that the closed-loop system with process model (4) with (42) and feedback controller (9) with (47), be nominally stable condition (19). This may be checked either using the perturbation index in (20) or by a straightforward stability analysis of the closed-loop.

6 Conclusions

This article has presented a framework and a constructive technique for designing feedback controllers for a class of practical spatially distributed systems. The design technique incorporates recent results for the optimal synthesis of controllers for spatially-invariant systems and extends traditional loop shaping techniques for dynamical systems into the two-dimensional frequency domain.

This approach allows a significant reduction in the amount of computation required for these typically large multivariable control systems and allows a better physical insight into the problem at the time of the design. The technique presented in this article has been used as the foundation of a software tool for the design of robust spatially distributed controllers for paper machines [37,40], and is currently running on several dozen industrial systems.

Acknowledgements

Financial support of this project from Honeywell Industry Solutions, the Natural Sciences and Engineering Research Council of Canada, and the University of British Columbia is gratefully acknowledged.

References

[1] R. Abraham and J. Lunze. Modelling and decentralized control of a multizone crystal growth furnace. *Int. J. Robust and Nonlinear Control*, 2:107–122, 1992.

[2] G. Ayres and F. Paganini. Convex synthesis of localized controllers for spatially invariant systems. *Automatica*, 38(3), March 2002.

[3] B. Bamieh, F. Paganini, and M. Dahleh. Distributed control of spatially invariant systems. *IEEE Trans. Automat. Contr.*, 47(7):1091–1107, July 2002.

[4] R.W. Brockett and J.L. Willems. Discretized partial differential equations: Examples of control systems defined on modules. *Automatica*, 10:507–515, 1974.

[5] R.Y. Chiang and M.G. Safonov. *Matlab Robust Control Toolbox - Version 2.* The MathWorks, Inc., 1997.

[6] R. D'Andrea and G.E. Dullerud. Distributed control of spatially interconnected systems. *IEEE Trans. Automat. Contr.*, submitted.

[7] P.J. Davis. *Circulant Matrices.* Wiley, New York, 1979.

[8] J.C. Doyle and G. Stein. Multivariable feedback design: Concepts for a classical/modern synthesis. *IEEE Trans. Automat. Contr.*, AC-26(1):4–16, February 1981.

[9] S.R. Duncan. *The Cross-Directional Control of Web Forming Processes.* PhD thesis, University of London, UK, 1989.

[10] S.R. Duncan and G.F. Bryant. The spatial bandwidth of cross-directional control systems for web processes. *Automatica*, 33(2):139–153, 1997.

[11] A.P. Featherstone, J.G. VanAntwerp, and R.D. Braatz. *Identification and Control of Sheet and Film Processes.* Springer, 2000.

[12] C.R. Fuller, S.J. Elliott, and P.A. Nelson. *Active Control of Vibration.* Academic Press, London, 1996.

[13] G.H. Golub and C.F. Van Loan. *Matrix Computations.* The Johns Hopkins University Press, Baltimore, 3rd edition, 1996.

[14] G.C. Goodwin, B.M. Carny, and W.J. Edwards. Analysis of thermal camber control in rolling mills. In *Proc. IFAC World Congress*, pages 160–164, Tallinn, USSR, 1990.

[15] D. Gorinevsky, T. Hyde, and C. Cabuz. Distributed shape control of lightweight space reflector structure. In *Proc. of IEEE Conference on Decision and Control*, pages 3850–3855, Orlando, FL, USA, December 2001.

[16] D.M. Gorinevsky. Honeywell opportunities in control of distributed micro electro-mechanical systems. In *Meeting on Distributed-Parameter System Control*, Cupertino, CA, USA, February 1999.

[17] D.M. Gorinevsky and G. Stein. Structured uncertainty analysis of robust stability for spatially distributed systems. In *Proc. of IEEE Conference on Decision and Control*, Sydney, Australia, December 2000.

[18] R.M. Gray. Toeplitz and circulant matrices: A review. *http://ee-www.stanford.edu/~gray/toeplitz.html*, 2001.

[19] W.P. Heath. Orthogonal functions for cross-directional control of web forming processes. *Automatica*, 32(2):183–198, 1996.

[20] M. Hovd, R.D. Braatz, and S. Skogestad. SVD controllers for $\mathcal{H}_2$-, $\mathcal{H}_\infty$- and μ-optimal control. *Automatica*, 33(3):433–439, 1997.

[21] M. Hovd and S. Skogestad. Control of symmetrically interconnected plants. *Automatica*, 30(6):957–973, 1994.

[22] D.W. Kawka. *A Calendering Model for Cross-Direction Control*. PhD thesis, McGill University, Montreal, Canada, 1998.

[23] K. Kristinsson and G.A. Dumont. Cross-directional control on paper machines using gram polynomials. *Automatica*, 32(4):533–548, 1996.

[24] C. Langbort and R. D'Andrea. Imposing boundary conditions for a class of spatially-interconnected systems. In *submitted to American Control Conference*, 2003.

[25] D.L. Laughlin, M. Morari, and R.D. Braatz. Robust performance of cross-directional control systems for web processes. *Automatica*, 29(6):1395–1410, 1993.

[26] W.S. Levine and M. Athans. On the optimal error regulation of a string of moving vehicles. *IEEE Trans. Automat. Contr.*, 11(3):355–361, August 1966.

[27] P. Lundstrom, S. Skogestad, and J.C. Doyle. Two-degree-of-freedom controller design for an ill-conditioned distillation process using μ-synthesis. *IEEE Trans. Contr. Syst. Technol.*, 7(1):12–21, January 1999.

[28] D. McFarlane and K. Glover. A loop shaping design procedure using $\mathcal{H}_\infty$ synthesis. *IEEE Trans. Automat. Contr.*, AC-37(6):759–769, June 1992.

[29] S. Mijanovic, G.E. Stewart, G.A. Dumont, and M.S. Davies. Stability-preserving modification of paper machine cross-directional control near spatial domain boundaries. In *IEEE Conf. Decision and Control*, Las Vegas, Nevada, USA, December 2002.

[30] A.V. Oppenheim and R.W. Schafer. *Discrete-Time Signal Processing*. Prentice Hall, New Jersey, 1989.

[31] F. Paganini. A recursive information flow system for distributed control arrays. In *Proc. of American Control Conf.*, pages 3821–3825, San Diego, CA, USA, June 1999.

[32] J. Reinschke. *$\mathcal{H}_\infty$ Control of Spatially Distributed Systems*. PhD thesis, Department of Engineering, University of Cambridge, England, 1999.

[33] J. Ringwood. Multivariable control using the singular value decomposition in steel rolling with quantitative robustness assessment. *Control Eng. Practice*, 3(4):495–503, 1995.

[34] S. Skogestad, M. Morari, and J.C. Doyle. Robust control of ill-conditioned plants: High-purity distillation. *IEEE Trans. Automat. Contr.*, 33(12):1092–1105, December 1988.

[35] S. Skogestad and I. Postlethwaite. *Multivariable Feedback Control: Analysis and Design*. Wiley, New York, 1996.

[36] G.D. Smith. *Numerical Solution of Partial Differential Equations: Finite Difference Methods.* Clarendon Press, Oxford, 3rd edition, 1985.

[37] G.E. Stewart. *Two Dimensional Loop Shaping: Controller Design for Paper Machine Cross-Directional Processes.* PhD thesis, Department of Electrical and Computer Engineering, University of British Columbia, Vancouver, Canada, 2000.

[38] G.E. Stewart. Analysis and design of boundary conditions for a spatially distributed control system. Technical report, Honeywell Industry Solutions, February 2001.

[39] G.E. Stewart, P. Baker, D.M. Gorinevsky, and G.A. Dumont. An experimental demonstration of recent results for spatially distributed control systems. In *submitted to Proc. of American Control Conf.*, Arlington, VA, USA, June 2001.

[40] G.E. Stewart, D.M. Gorinevsky, and G.A. Dumont. Feedback controller design for a spatially-distributed system: The paper machine problem. *to appear in IEEE Trans. Contr. Syst. Technol.*, 2003.

[41] W.A. Strauss. *Partial Differential Equations: An Introduction.* Wiley, New York, 1992.

[42] K. Zhou, J.C. Doyle, and K. Glover. *Robust and Optimal Control.* Prentice Hall, New Jersey, 1996.

A Familiar PDEs

A wide variety of discrete spatially distributed systems may be represented by a low-order transfer function using the structure (3), (4). This representation arises in the explicit methods of numerical solution for partial differential equations by finite-difference approximation. For example, the explicit solution for the heat (or diffusion) equation, $\partial y/\partial t = \partial^2 y/\partial x^2$, is often discretized with $m_b = 1$, $m_a = 1$ in (4),

$$y(t) = u(t-1) + A \cdot y(t-1), \tag{A.1}$$

with homogeneous Dirichlet boundary conditions the matrix $A = \mathcal{T}(\bar{a}, n)$ with $\bar{a} = [2r-1, -r]$ and $0 < r \leq 1/2$ is required for a stable solution [36,41].

The explicit solution for the undamped, second order wave equation, $\partial^2 y/\partial t^2 = \kappa^2 \partial^2 y/\partial x^2$, is often discretized by (3), (4) with $m_b = 1$ and $m_a = 2$ in the update equation,

$$y(t) = u(t-1) + A_1 \cdot y(t-1) + A_2 \cdot y(t-2) \tag{A.2}$$

with homogeneous Dirichlet boundary conditions the matrices $A_1 = \mathcal{T}(\bar{a}_1, n)$ and $A_2 = \mathcal{T}(\bar{a}_2, n)$ with $\overline{a}_1 = [2(r-1), -r]$ and $\overline{a}_2 = [1, 0]$ respectively. For stability, the solution requires $0 < r \leq 1$ (see [36,41]).

B Fourier Matrices

The complex Fourier matrix may be constructed [3] as follows [21],

$$\mathcal{F}^H = \frac{1}{\sqrt{n}}[m_1 \; m_2 \; \cdots \; m_n] \tag{B.1}$$

where the vectors $m_k \in \mathcal{C}^{n\times 1}$ are given by,

$$m_k = [1 \; v_k \; v_k^2 \; \cdots \; v_k^{n-1}]^T, \qquad v_k = e^{2\pi(k-1)i/n} \tag{B.2}$$

In other words, the k^{th} row of $\mathcal{F}$ contains the k^{th} spatial harmonic and has frequency ν_k. The complex Fourier matrix $\mathcal{F} \in \mathcal{C}^{n\times n}$ in (B.1) may then be used to diagonalize any $n \times n$ circulant matrix,

$$A = \mathcal{F}^H \Sigma_A \mathcal{F}, \qquad \Sigma_A = \mathrm{diag}\{a(\nu_1), \ldots, a(\nu_n)\} \tag{B.3}$$

The subset of circulant *symmetric* matrices may be diagonalized with a pure real Fourier matrix. The real Fourier matrix F is constructed from the complex Fourier transform matrix $\mathcal{F}$ in (B.1) by the following unitary operations,

$$\begin{aligned} F(1,:) &= \frac{1}{n}[1, \; 1, \ldots, 1] \\ F(k,:) &= \frac{1}{\sqrt{2}}\left(\Im m[\mathcal{F}(k,:)] - \Im m[\mathcal{F}(n+2-k,:)]\right) \\ F(n+2-k,:) &= \frac{1}{\sqrt{2}}\left(\Re e[\mathcal{F}(k,:)] + \Re e[\mathcal{F}(n+2-k,:)]\right) \end{aligned} \tag{B.4}$$

for $k = 2, \ldots, p$, where $p = (n+1)/2$ if n is odd and $p = n/2$ if n is even. The j^{th} row of F contains the j^{th} spatial harmonic and has frequency $\nu_j = 2\pi(j-1)/n$. The real Fourier matrix F is unitary, satisfying the property $F^T F = I$.

More intuitively, the rows of the real Fourier matrix F in (B.4) may be re-written in terms of the familiar trigonometric functions,

[3] The unitary, complex Fourier matrix $\mathcal{F}$ may be created, for example, using the MATLAB command $\mathcal{F}$ = fft(eye(n))/sqrt(n).

$$F(j,k) = \begin{cases} \sqrt{\frac{1}{n}} & j = 1 \\ \sqrt{\frac{2}{n}} \cdot \sin[(k-1)\nu_j] & j = 2, \ldots, p \\ \sqrt{\frac{2}{n}} \cdot \cos[(k-1)\nu_j] & j = p+1, \ldots, n \end{cases} \tag{B.5}$$

C Proof of Theorem 4

Defining the arrays,

$$\hat{\mathbf{c}}_\mathbf{r} := [\hat{c}_r(\nu_1), \ldots, \hat{c}_r(\nu_n)]^T, \qquad \hat{\mathbf{c}} := [\hat{c}(\nu_1), \ldots, \hat{c}(\nu_n)]^T \tag{C.1}$$

allows (33) to be written in terms of a standard finite dimensional least squares optimization problem with J in (33) given by,

$$J = \|\hat{\mathbf{c}}_\mathbf{r} - \hat{\mathbf{c}}\|_2^2 \tag{C.2}$$

where the vector norm $\|x\|_2 = (x^T x)^{1/2}$. From [7,18] the eigenvalues of the symmetric circulant matrix $\hat{C}_r$ in (32) are given by,

$$\hat{c}_r(\nu_j) = c_1 + \sum_{i=2}^{n_c} c_i \cdot \cos[(i-1)\nu_j] \tag{C.3}$$

and may be written using (C.1) in terms of the matrix equation

$$\hat{\mathbf{c}}_\mathbf{r} = A \cdot \bar{c}, \tag{C.4}$$

with $\bar{c} = [c_1, \ldots, c_{n_c}]^T$ and

$$A = \begin{bmatrix} 1 & 2\cos[\nu_1] & 2\cos[2\nu_1] & \cdots & 2\cos[(i-1)\nu_1] \\ \vdots & \vdots & \vdots & & \vdots \\ 1 & 2\cos[\nu_n] & 2\cos[2\nu_n] & \cdots & 2\cos[(i-1)\nu_n] \end{bmatrix} \tag{C.5}$$

Combining (C.2) and (C.4) gives,

$$\|\hat{\mathbf{c}}_\mathbf{r} - \hat{\mathbf{c}}\|_2^2 = \|A \cdot \bar{c} - \hat{\mathbf{c}}\|_2^2 \tag{C.6}$$

The optimal solution of (C.6) for invertible $A^T A$ is given (for example in Chapter 5, [13]) by,

$$\bar{c}_{opt} = (A^T A)^{-1} A^T \cdot \hat{\mathbf{c}} \tag{C.7}$$

Due to the orthogonality of the columns of A, the $n_c \times n_c$ matrix $A^T A$ is diagonal with elements,

$$A^T A = \text{diag}\{n, 2n, \ldots, 2n\} \tag{C.8}$$

The coefficients (34) are then computed from substitution of (C.1), (C.5), (C.8), into (C.7).

$\diamondsuit$